# Numerical simulations of crashworthiness performance of multi-cell structures considering damage evolution criteria

*Quirino* Estrada[1*], *Dariusz* Szwedowicz[2], *Alejandro* Rodriguez-Mendez[3], *Jesús* Silva-Aceves[1], *Javier S.* Castro[1], *Lara C.* Wiebe[1], *Elifalet* Gonzalez[1], *Julio* Vergara-Vazquez[2] and *Andrea E.* Chavez[1]

[1]Institute of Technology and Engineering, Autonomous University of Juarez City (UACJ), Ciudad Juárez, Chihuahua, México.
[2]Mechanical Engineering Department, National Centre for Research and Technological Development, Cuernavaca, Morelos, México.
[3]Department of Mechanical Engineering, University of California, Berkeley, CA 94720, USA.

**Abstract.** In this paper finite element software Abaqus was used to analyse the effect of cross-sectional shape on the crashworthiness performance of multi-cell profiles. An emphasis was placed on the modelling of the damage initiation criteria and its evolution during the crash event. The structures evaluated included square and circular multi-cell cross-sections fabricated with aluminium alloy EN AW-7108 T6. During the crash simulations, the structures were subjected to axial impact loads using a 500-kg rigid body striker with an initial velocity of 10 m/s. Accordingly to our results, profiles with circular cross-section base presented better crashworthiness performance than square profiles. An increase in crush force efficiency to 36.9% and specific energy to 35.4% was observed when a circular cross-section has been reinforced in the transversal and longitudinal directions. Finally, it was corroborated that the addition of the damage initiation criteria allowed for more reliable crash simulations of the structures.

## 1 Introduction

The use of thin-walled structures, as energy absorbers increases, improves the safety of passenger during car collisions [1]. Based on crashworthiness requirements, the thin-walled structures should minimise the peak load at the beginning of the crash event, maximise the energy absorption by plastic deformation and minimise weight [2]. Structures made of aluminium alloys are widely implemented in the automotive industry to satisfy the above requirements. Due to the lightness of aluminium alloys relative to steel, the total weight of a vehicle can be reduced by 28% [3]. This allows to reduce fuel consumption and consequently the emission of harmful contaminant agents into the atmosphere [4]. Several numerical and experimental studies have been conducted with the purpose of maximising the crashworthiness performance of thin-walled structures [5,6]. Hence, the study of multi-cell structures is developing. A multi-cell profile is obtained when a single cross-section is reinforced by plates at different angle of connectivity. Nia and Parpasour [7] conducted a comparative study of energy absorption of single and multi-cell structures. Several cross-sections based on triangular, square, hexagonal and octagonal shape were analysed. They observed that multi-cell profiles showed better energy absorption in comparison to single-cell profiles. Likewise, larger energy absorption per unit mass was obtained by hexagonal and octagonal multi-cell configurations. This observation was confirmed by Pirmohammad and Marzdashti [8] who analysed the energy absorption capacities of single and multi-cell profiles under axial and oblique quasi-static load. From their numerical results, it was determined that multi-cell structural members with an inner tube had larger energy absorption ($E_a$), notably when the inner and outer profiles were at a scale of 0.5. They found that multi-cell profiles with circular cross-sections allowed the best $E_a$ performance. Tang et al [9] determined that the crashworthiness characteristics of circular multi-cell configurations depends mainly on the thickness and the number of cells along the radial and transversal directions. They concluded that the double layer cylindrical multi-cell structure was the most suitable to increase crashworthiness performance. Continuing with circular multi-cell profiles, Ahmed et al. [10] investigated the energy absorption capacities of several tube arrangements with curved stiffeners under dynamic axial load. Their numerical results evidenced the effectiveness of curved stiffeners to improve the energy absorption of columns. However, relative to circular single-cell profiles, bi-tubular arrangement with curved stiffeners showed better stability to the lowest peak load. On the other hand, to get reliable numerical results some researches have added theoretical damage models into their simulations [11-13]. Therefore, Hooputra et al. [14] presented a compressive macroscopic strain and stress model. The failure mechanism, considered in this approach, involves ductile, shear and necking instabilities. The effectiveness of this approach was shown by comparing numerical results with experimental data for a double chambered profile under

* Corresponding author: quirino.estrada@uacj.mx

axial compression and three point bending tests. Based on this approach Estrada et al. [13] evaluated the effect of circular discontinuities on the crashworthiness performance of square profiles under an impact load. In all cases, the addition of discontinuities improved the energy absorption capacity of the square profiles relative to a structure without holes. However, the best Ea performance equal to 17.61 kJ has been obtained when the holes were drilled at the top of the walls of the structure. As mentioned, significant efforts have been put to get more accurate numerical results, however the use of damage criteria and its evolution were less reported on numerical simulation of multi-cell structures. The current paper analyses the effect of cross-sectional shape on the crashworthiness response of multi-cell profiles. For this purpose, we considered multi-cell structures made with aluminium alloy EN AW-7108 T6 under a dynamic compression test. We tested multi-cell cross-sections with square and circular shapes. In order to get a reliable outcome, great emphasis was placed on the modelling of damage and its evolution.

### 1.1 Crashworthiness indicators

The parameters used to estimate the energy absorption capabilities of thin-walled structure should not dependent on geometry, material and mass. The energy absorption due to elastic and plastic deformation can be calculated from Equation 1. This refers to work done by the external force (*F*) along to the displacement ( $\delta$ ).

$$E_a = \frac{1}{2}\sum_{i}^{n-1}\left[\left(F(\delta)_{i+1} + F(\delta)_i\right)\cdot\left(\delta_{i+1} - \delta_i\right)\right] \quad (1)$$

The rate of the energy absorbed ($E_a$) to the displacement is described as the mean crush force ($P_m$) and it is calculated from:

$$P_m = E_a \big/ \delta \quad (2)$$

The crush force efficiency (CFE) allows better comprehension of crashworthiness performance of structures. This parameter is given by Eq. 3. A value close to 1 indicates the optimal performance of the columns.

$$CFE = P_m \big/ P_{\max} \quad (3)$$

Also, when the structure has different masses (m), we define the specific energy absorption (SEA) by:

$$SFA = S_a \big/ m \quad (4)$$

### 1.2 Damage criteria and its evolution

Finite element simulations are widely used to analyse the mechanical behaviour of structures. However, when these structures are subjected to dynamic loads, the mechanical behaviour becomes increasingly complex. Phenomena such as failure and fracture by ductile and shear mechanisms are presented. In order to correctly capture the behaviour of the structures, the article considers the ductile and shear damage initiation criteria proposed by Hooputra et al. [14] available in Abaqus/explicit. Experimental data for all models was obtained from [14,15] for aluminium alloy EN AW-7108 T6 and is shown in the Table 1. The ductile criterion, used in the simulations, assumes the equivalent plastic strain at the onset of damage to be a function of stress triaxiality and strain rate. Analogously, the shear criterion was specified by considering the equivalent plastic strain at the onset of shear damage to be a function of shear stress ratio and strain rate. Simplified analytical expressions presented by Hooputra et al. [14,15] are presented in Eqs. (5) and (6) for ductile and shear criteria, respectively.

$$\bar{\varepsilon}_D^{pl}\left(\eta, \bar{\varepsilon}^{pl}\right) = \frac{\varepsilon_T^+ \sinh\left[k_0\left(\eta^- - \eta\right)\right] + \varepsilon_T^- \sinh\left[k_0\left(\eta - \eta^+\right)\right]}{\sinh\left[k_0\left(\eta^- - \eta^+\right)\right]} \quad (5)$$

$$\bar{\varepsilon}_S^{pl}\left(\theta_S, \bar{\varepsilon}^{pl}\right) = \frac{\varepsilon_S^+ \sinh\left[f\left(\theta_S - \theta_S^-\right)\right] + \varepsilon_S^- \sinh\left[f\left(\theta_S^+ - \theta_S\right)\right]}{\sinh\left[f\left(\theta_S^+ - \theta_S^-\right)\right]} \quad (6)$$

where $\varepsilon_T^+$ and $\varepsilon_T^-$ are equivalent plastic strains for equibiaxial tensile and equibiaxial compressive deformation, respectively. For isotropic materials, the stress triaxility in equibiaxial tensile deformation ( $\eta^+$ ) is equal to 2/3, and for equibiaxial compression deformation, $\eta^-$ is -2/3. In Abaqus, $\eta$ is defined as the ratio of the equivalent mean stress to the Misses equivalent stress. The values of $k_{0,}\varepsilon_T^+$ and $\varepsilon_T^-$ were taken from [15]. For Eq. (6), $\varepsilon_S^+$ is the equivalent plastic strain at the shear damage initiation for equibiaxial tensile and $\varepsilon_S^-$ corresponds to equibiaxial compressive deformation. $\theta_S^+$ and $\theta_S^-$ are the values of $\theta_S$ at $\eta = \eta+$ and $\eta = \eta-$, respectively. In this case, $\theta_S = \dfrac{1 - k_s\eta}{\phi}$ where $\phi = \tau_{\max} \big/ \sigma_{eq}$. The parameters $k_{s0}\varepsilon_S^+\varepsilon_S^-$ and $f$ are determined experimentally.

**Table 1.** Failure parameters for aluminium alloy EN AW-7108 T6 at a strain rate of 250 s-1 [14, 15].

| Parameter | Ductile failure parameters | Shear failure parameters |
|---|---|---|
| $\varepsilon_T^2$ | 0.44 | - |
| $\varepsilon_T^-$ | 1.494 | - |
| $k_0$ | 8.6304 | - |
| $\varepsilon_S^+$ | - | 0.35 |
| $\varepsilon_S^-$ | - | 1.2 |
| $f$ | - | 2.05 |
| $k_s$ | - | 0.3 |

## 2 Validation of numerical model

To evaluate the effectiveness of damage criteria on the progressive damage of a structure, a numerical model was developed using Abaqus/explicit. For this purpose, some guidelines given in [15] were considered. The discrete model consisted of a double-chambered profile under axial compression impact load. The profile was made of aluminium EN AW-7108 T6, with length L~396.5 mm, height H=68 mm, width W=95 mm and thickness t = 2.5 mm. The impact was done by a rigid body with a mass of 500 kg. The velocity applied was 10 m/s. We used a Young modulus of 70 GPa, Poisson ratio of 0.33 and density of 2700 kg/m$^3$. Likewise, ductility, shear, and Müschenborn-Sonne forming limit diagram (MSFLD) damage initiation criteria with evolution were considered. An element sized 5 mm was used to discretise the double-chambered structure. This value was validated using experimental data from [14,15]. The model and boundaries conditions are shown in the Figure1.

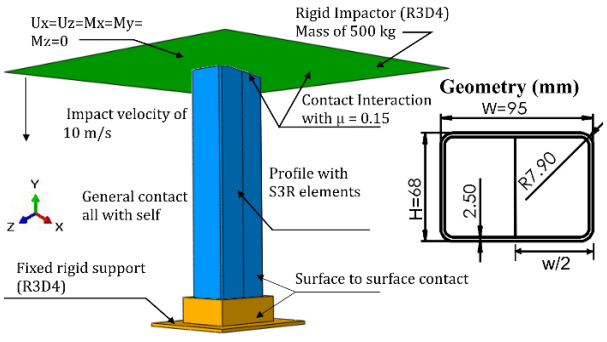


**Fig. 1.** Discrete model and boundary conditions.

Numerical results were compared with experimental data obtained by Hooputra et al. [14,15] and are presented in the Figure 2. The effect of damage modelling was studied, as well as its evolution, using a second numerical model without damage criteria. From the force vs displacement curve a $P_{max}$ ~180 kN was computed; this value represented a difference of 5% relative to experimental data. The model with damage and its evolution properly represented the mechanical behaviour of the structure, especially after $P_{max}$ was reached. At that point, a drop-in crushing force was registered, and the fracture of the profile could be visible. The opposite case was obtained by the model without damage criteria, where no cracks and progressive damage were observed (see in the Figure 3).

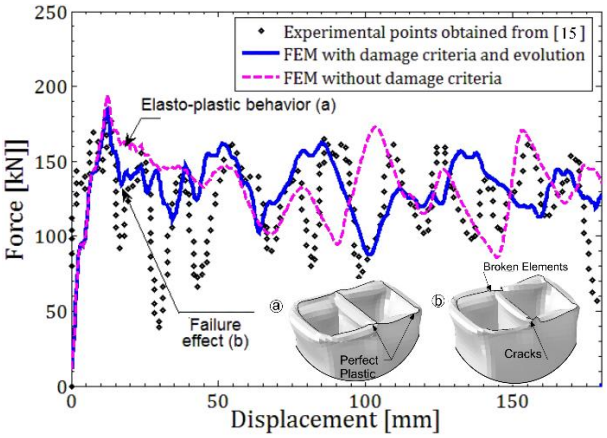


**Fig. 2.** Force vs displacement curves for the double-chambered profile.

Figure 3 presents the final deformation state of the structure, where it can be observed how the damage criteria and its evolution effectively reproduce the post-failure behaviour of the structure.

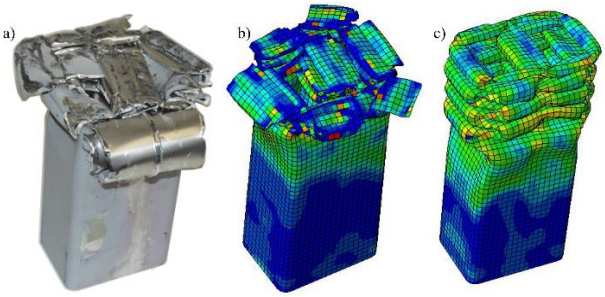


**Fig. 3.** Final deformation state, where: a) experimental [14,15], b) numerical with damage criteria and c) numerical without damage criteria.

Comparing the numerical and experimental results, the feasibility of the discrete model was validated. Thus, we can proceed to the crashworthiness analysis of multi-cell profiles.

## 3 Finite Element simulations

The article analyses the effect of cross-section on the crashworthiness response of multi-cell profiles. For this purpose, six structures with square and circular cross-sections were selected. The structures were made of aluminium alloy EN AW-7108 T6 with a length of 400 mm. The conditions of the numerical test were the same as those described in Section 2. The evaluated geometry of the specimens is displayed in the Figure 4 and the Table 2.

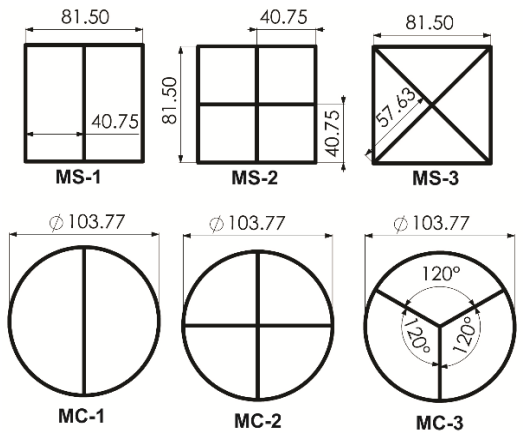


**Fig. 4.** Cross-sections analysed (mm).

**Table 2.** Details of multi-cell structures.

| Code | Geometric base | Thickness (mm) | Length (mm) | Mass (gr) |
|---|---|---|---|---|
| MS-1 | Square | 2.5 | 400 | 1100 |
| MS-2 | Square | 2.08 | 400 | 1100 |
| MS-3 | Square | 1.83 | 400 | 1100 |
| MC-1 | Circular | 2.37 | 400 | 1100 |
| MC-2 | Circular | 1.91 | 400 | 1100 |
| MC-3 | Circular | 2.12 | 400 | 1100 |

## 4 Results and Discussion

### 4.1 Square multi-cell profiles

Force vs displacement curves were obtained for all evaluated structures. To get a real comparison between profiles, the curves were delimitated to 160 mm. From the Figure 5, an approximate value of $P_{max}$ of 350 kN can be interpreted. Three different behaviours were observed. The MS-3 profile showed the best stability to deformation. The curve presented straight zones which indicated a controlled deceleration. The opposite case was observed from the MS-2 structure.

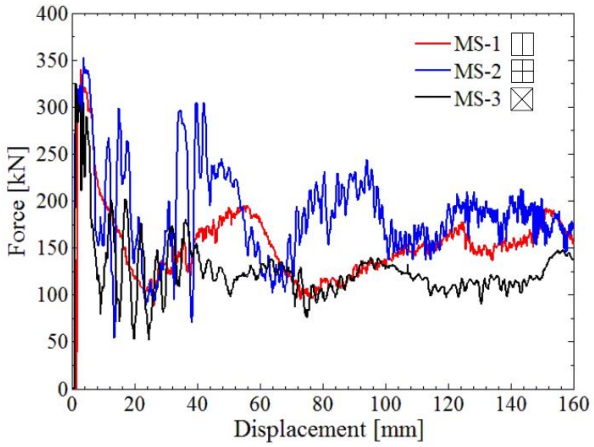


**Fig. 5.** Force vs displacement curves for square multi-cell columns.

The modelling of damage and its evolution becomes important when the final deformation of the structure is required with accuracy. Figure 6 shows the final deformation state of the profiles at 160 mm of displacement. In all cases, the failure and fracture of some elements located on the corners and ribs were observed. The deformation pattern of the columns was characterised by a symmetrical deformation mode described in [1].

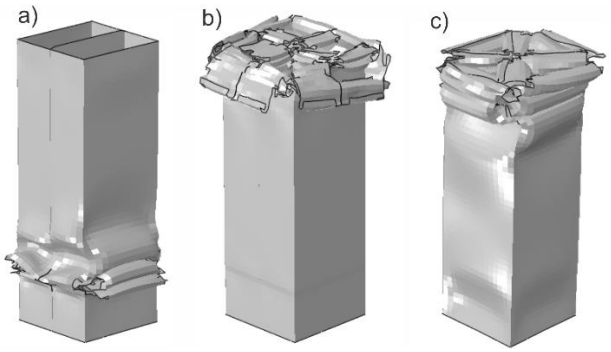


**Fig. 6.** Final deformation state for square multi-cell columns.

The mode of collapse and energy absorption performance depended on the failure of the structure by shear and ductile mechanism. Figure 7 shows the ductile damage initiation indicator. Failure by tension and compression effects were registered on some elements of the outer cylindrical surface on both the profile and the ribs. A value of 1 indicated that damage which has been initiated.

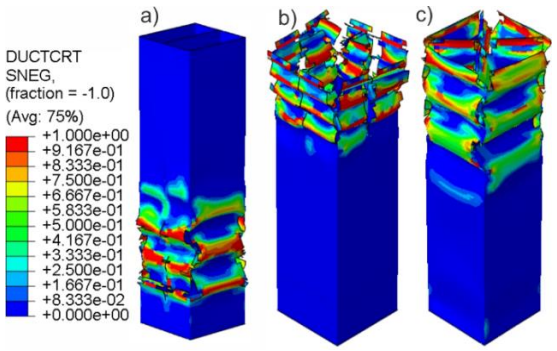


**Fig. 7.** Ductile damage initiation indicator.

Failure by shear band mechanism was more visible than failure by ductile effects. During the plastic wrinkle formation, failure by shear mechanism was observed on some elements used to form conical and toroidal surfaces. Additionally, shear effects were observed on the T joint formed by the ribs with the profile as seen in the Figure 8.

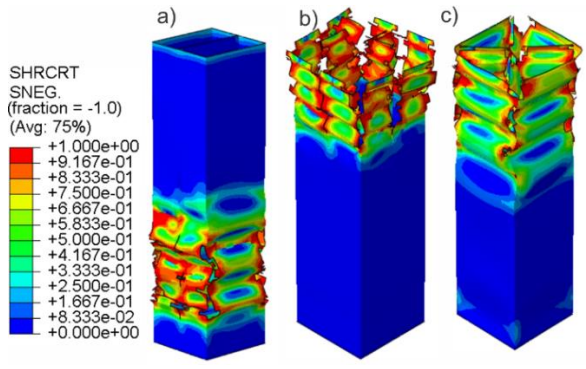


**Fig. 8.** Shear damage initiation indicator.

A summary of the results calculated for 160 mm of displacement is presented in the Table 3. An increase on energy absorption ($E_a$) in the rage of 21.66 to 39.31% was obtained for MS-1 and MS-2, relative to the worst energy absorption performance (MS-3). Since all structures had the same mass, the best energy absorption per unit of mass (SEA) and CFE value was for the MS-2 profile, with a value of 25.54 J/gr and 0.497, respectively. This condition indicated that the cross-section of this profile contributed to a better collapse mode of the structure. Thus, a large quantity of energy deformation was obtained (28.10 kJ).

**Table 3.** Summary of numerical results I.

| Code | $P_{max}$ (kN) | $P_m$ (kN) | $E_a$ (kJ) | SEA (J/gr) | CFE |
|---|---|---|---|---|---|
| MS-1 | 339.70 | 153.37 | 24.54 | 22.30 | 0.451 |
| MS-2 | 353.01 | 175.62 | 28.10 | 25.54 | 0.497 |
| MS-3 | 325.60 | 126.06 | 20.17 | 18.33 | 0.387 |

Moreover, it was confirmed that the energy absorption capabilities of profiles were mainly determined by the arrangement of the ribs in the profile, more than their number.

### 4.2 Circular multi-cell profiles

The crashworthiness performance of circular multi-cell profiles was obtained by the crash force vs displacement curves and they are presented in the Figure 9. The comparison of curves was realised at 160 mm of displacement. The curves were characterised by a controlled deformation along the crushing process. Thus, no abrupt changes in acceleration were registered. The curves presented similar mechanical behaviour, however the formation of wrinkles was out of phase, caused by the arrangement of the ribs in the cross section.

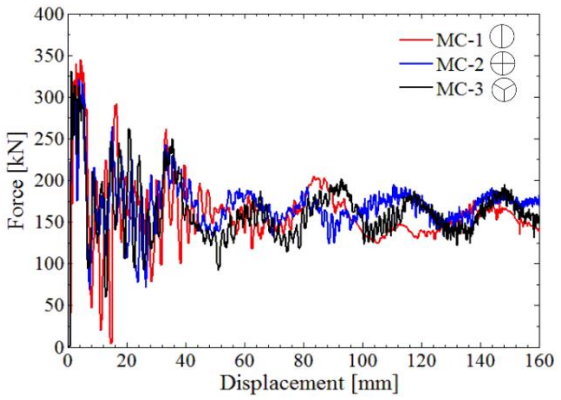


**Fig. 9.** Force vs displacement curves for circular multi-cell columns.

Figure 10 shows the final deformation state at a displacement of 160 mm. For all cases, the plastic deformation occurred at the top of the columns and was propagated in the downward direction. Even though the damage initiation criteria and its evolution modified the deformation mode of the structure, the columns were deformed in concertina and diamond mode. The fracture was located on the joints formed by the ribs and the outer profile. The largest damage effects were obtained by the MC-2 profile.

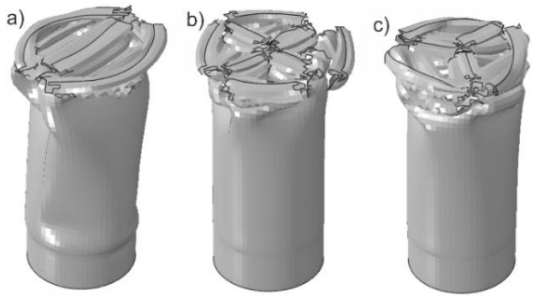


**Fig. 10.** Final deformation state for circular multi-cell columns.

The collapse mode was mainly determined by the cross-section arrangement and by failure of the elements. Thus, it was confirmed that the failure of circular multi-cell columns was due to ductile fracture (void nucleation, coalescence and growth) and shear band fracture. Figure 11 and 12 show ductile and shear damage initiation criteria, respectively, where a value of 1 indicates that the criterion has been satisfied. For all cases, the ductile criterion was met by some elements used to form the hinge line during the formation of the triangular folds. Meanwhile, the shear criterion was satisfied on elements near the T joint.

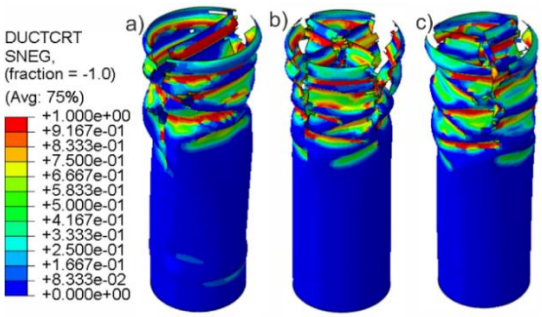


**Fig. 11.** Ductile damage initiation indicator.

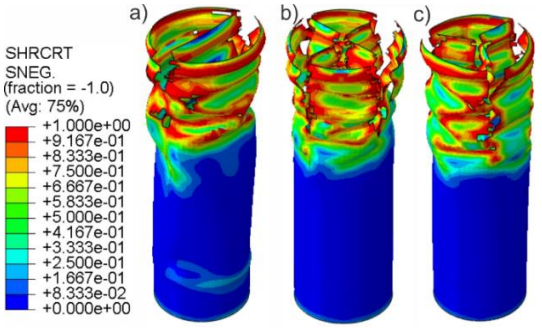


**Fig. 12.** Shear damage initiation indicator.

The addition of damage models and its evolution into the discrete models contributed to determine the correct mechanical behaviour of the structures. The numerical results are presented in the Table 4. The best energy absorption ($E_a$) was obtained by MC-2 profile (27.56 kJ) due to its larger deformation compared to all other profiles. Likewise, a greater external work was required to deform the walls of the column. The increase of the number of ribs contributed to improve the $E_a$ performance in a rage of 1.65-6.88% relative to the worst $E_a$ performance. The most favourable cross-section is the MC-2 profile, as demonstrated for higher values of SEA (24.83J/gr) and CFE (0.53).

**Table 4.** Summary of numerical results II.

| Code | $P_{max}$ (kN) | $P_m$ (kN) | $E_a$ (kJ) | SEA (J/gr) | CFE |
|---|---|---|---|---|---|
| MS-1 | 344.80 | 159.75 | 25.56 | 23.23 | 0.46 |
| MS-2 | 321.01 | 170.75 | 27.32 | 24.83 | 0.53 |
| MS-3 | 331.10 | 162.37 | 25.98 | 23.61 | 0.49 |

### 4.3 Comparing results

To understand the direct effect of the cross-section on the crashworthiness performance, a comparative analysis of SEA and CFE is shown in Figures 13 and 14, respectively. We observed the increase of SEA when the cross-sections have been reinforced in the longitudinal and traversal directions (MS-2 and MC-2). However, the best SEA performance of 25.54 J/gr was obtained by the MS-2 profile. That value represented the increase of 39.3% relative to the MS-3 profile. The worst CFE behaviour (18.33 J/gr) was obtained by the MS-3 structure.

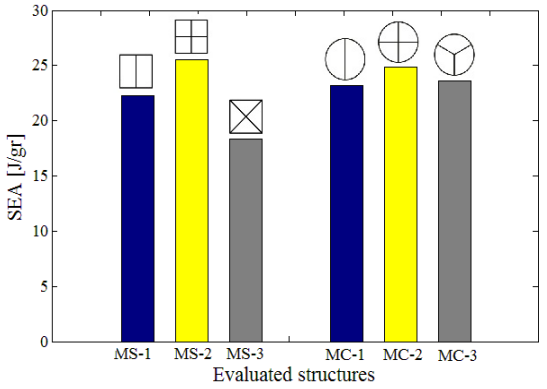


**Fig. 13.** SEA values of the structures evaluated.

A comparison of CFE value is presented in the Figure 14. A value close to 1 indicates the most desirable CFE value. The improvement of 36.95% was obtained for the MC-2 structure relative to the lowest CFE. For this case a maximum value of CFE around 0.58 was obtained. This value suggested a reasonable low peak load with a large quantity of energy absorption when the circular multi-cell cross-section has been reinforced in the transversal and longitudinal direction. In general, circular multi-cell profiles present better CFE performance than square columns in a range of 21.05-36.95%.

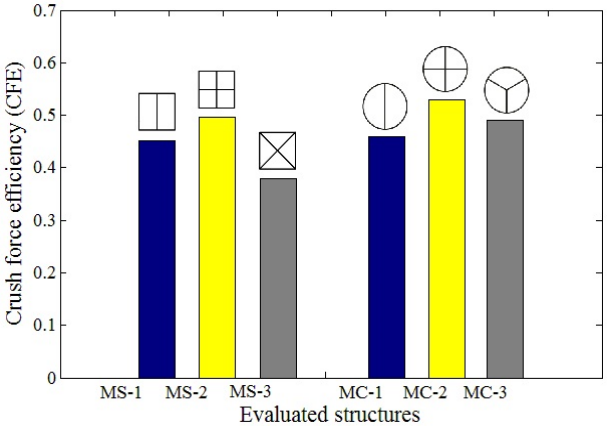


**Fig. 14.** CFE values of the structures evaluated.

From the Figure 13 and 14 the best crashworthiness performance was obtained for the circular multi-cell profile MC-2. Thus, this kind of cross-section arrangement should be considered in the design of energy absorption systems as an effective and low-cost solution for the automotive engineers.

## 5 Conclusions

A numerical study was conducted to evaluate the effect of the cross-sectional shape on the crashworthiness performance of multi-cell profiles with certain emphasis put on the modelling of progressive damage. For all cases, the use of ribs allowed better stability of the structure, minimising the buckling effect and maximising the energy absorption capacity. Regarding square multi-cell profiles, an improvement of CFE

(28.57 %) and SEA (39.31%) was obtained when the cross-section has been reinforced by 4 ribs in the transversal and longitudinal directions. That condition was also valid for circular multi-cell profiles, where an increase of $E_a$ of 6.88% relative to MC-1 was obtained by the MC-2 profile. Of all the multi-cell cross sections, the circular shapes showed better crashworthiness performance when compared with square cross sections. The best performance was obtained by the MC-2 profile with a SEA value of 24.83 J/gr and CFE value of 0.53. It was determined that the crashworthiness performance of the structures depended mainly on the geometric base of the cross-section followed by the arrangement of the ribs and finally by the number of ribs. Likewise, it was confirmed the accuracy of numerical results to incorporate damage initiation criteria and its evolution. Finally, the MC-2 profile should be considered in the design of energy absorption devices to reduce the injuries to passenger during car collisions.

This work was supported by the Programa para el Desarrollo Profesional Docente para el tipo superior (PRODEP), through project No. PROMEP/103.5/16/10473, UACJ-PTC-349.

## References

1. Q. Estrada, D. Szwedowicz, T. Majewski, E. Martinez, A. Rodriguez-Mendez, EIN-Maintenance and Reliability **18** (2016).
2. Q. Estrada, D. Szwedowicz, T. Majewski, M Baltazar, C Cortes, T Majewski, CA Estrada, Int. J Adv. Manuf. Technol. **84** (2016).
3. B. Simhachalam, K. Srinivas, R. Lakshmana, Int. J. Crashworthiness **19** (2014).
4. S. Wenlong, C. Xiaokai, W. Lu, Energy Proc. **88** (2016).
5. D. Szwedowicz, Q. Estrada, C. Cortes, J. Bedolla, G. Alvarez, F. Castro, Lat. Am. J. Solids Struct. **11** (2014).
6. M. Ferdynus, EIN-Maintenance and Reliability **15** (2013).
7. A.A Nia, M. Parsapour, Thin-Walled Struct. **74** (2014).
8. S. Pirmohammad, S. E. Marzdashti, Thin-Walled Struct. **108** (2016).
9. Z. Tang, S. Liu, Z. Zhang, Thin-Walled Struct. **62** (2013).
10. N. Ahmed, P. Xue, M. Kamran, N. Zafar, A. Mustafa, M.S. Zahran, Lat. Am. J. Solids Struct. **14** (2017).
11. J.S. Qiao, J. H. Chen, H. Y. Che, Thin-Walled Struct. **44** (2006).
12. J. Marzbanrad, A. Keshavarzi, F. H. Aboutalebi, Int. J. Crashworthiness **19** (2014).
13. Q. Estrada, D. Szwedowicz, J. Silva-Aceves, T Majewski, J. Vergara, A. Rodriguez-Mendez, Int. J. Mech. Sci. **131-132** (2017).
14. H. Hooputra, H. Gese, H. Dell, H. Werner Int. J. Crashworthiness **9** (2004).
15. Abaqus 6.10. Analysis User's Manual. (Dessault Systémes, 2010).